Desalination and Water Treatment
www.deswater.com

doi: 10.5004/dwt.2019.23192

137 (2019) 371–380
January

Photocatalytic degradation of aqueous methyl orange using a novel $Ag/TiO_2/Fe_2O_3$ photocatalyst prepared by UV-assisted thermal synthesis

Mohsen Nasirian, Mehrab Mehrvar*

Department of Chemical Engineering, Ryerson University, 350 Victoria Street, Toronto, ON, Canada, Tel. +1 (416) 979-5000 Ext. 6555; Fax: +1 (416) 979-5083; emails: mmehrvar@ryerson.ca (M. Mehrvar), mohsen.nasirian@ryerson.ca (M. Nasirian)

Received 1 May 2018; Accepted 24 September 2018

ABSTRACT

The aim of this study is to develop a novel photocatalyst doped by a noble metal onto two semiconductor oxides for the applications of photocatalytic wastewater treatment. An alternative preparation method of UV-assisted thermal synthesis is used to synthesize this photocatalyst. The two photocatalysts, Fe_2O_3 and TiO_2, were combined with different mass ratios of Fe:TiO_2 followed by doping the synthesized Fe_2O_3/TiO_2 with a silver ion with different mass ratios of Ag:TiO_2 to produce the novel photocatalyst $Ag/TiO_2/Fe_2O_3$. Scanning electron microscopy coupled with energy-dispersive X-ray spectroscopy is employed to evaluate the formation, the morphology, and the elemental analysis of the composite photocatalyst. The phase and the crystal structure of the new composites are investigated by X-ray diffraction. The specific surface area of all photocatalysts is analyzed based on the Brunauer–Emmett–Teller method by adsorption of nitrogen gas at 77 K. Removal of methyl orange is used to examine the photocatalytic degradation efficiency of the photocatalysts. Results indicate that the specific surface area of the $Ag/TiO_2/Fe_2O_3$ photocatalyst was significantly increased and the photocatalytic activity of the new photocatalyst was enhanced for the degradation of aqueous methyl orange. The new composite has the potential to absorb light at a higher wavelength in the visible region where the redshift occurs. By applying the $Ag/TiO_2/Fe_2O_3$ photocatalyst with a mass ratio of 0.01 Ag:TiO_2 and 0.01 Fe:TiO_2, the maximum degradation of methyl orange reaches to 89.5% and 95.5% under UV-A radiation and natural sunlight, respectively. Diffractograms confirm that the substitutions occur in the crystal lattice of the main photocatalyst.

Keywords: $Ag/TiO_2/Fe_2O_3$ photocatalyst; Photocatalysis; Metal doping; UV-assisted thermal synthesis; Methyl orange

1. Introduction

Recently, many studies have been devoted to the destruction of organic materials in wastewater by advanced oxidation processes (AOPs). This is mainly because AOPs can entirely eradicate organics [1–5]. AOPs are based on the generation of hydroxyl radicals ($HO^{\bullet}$), which can oxidize almost all organic materials in wastewater. Furthermore, $HO^{\bullet}$, with an oxidation potential of 2.8 eV, is the strongest oxidant after fluorine (3.06 eV) [6–12]. As one of the AOPs, photocatalysis is a promising method of eradicating almost all types of organics in wastewater. Among all photocatalysts, TiO_2 is considered as an efficient photocatalyst for the removal of organics in wastewater. Despite all advantages of TiO_2, there are two major limitations in its photocatalytic activity including its activation only in the ultraviolet range below 387 nm (3.2 eV) and a high rate of electron–hole recombination [5,13]. The photocatalytic efficiency of a photocatalyst depends on how well the electron–hole pair recombination could be prevented.

One of the main foci of the heterogeneous photocatalysis has been on its photoactivity on the visible region since majority of photocatalysts are photoactive only in the UV region. There are several studies on doping and deposition of metals (e.g., Au, Ag, Pt, Rh, Ru, Y, La, Mn, V, and Fe)

* Corresponding author.

or nonmetals (e.g., N, S, P) onto TiO_2 [14–21] to improve the photoactivity of photocatalysts in the visible region. In addition, there are studies on dye adsorption/sensitization, various hybrid composites or combining semiconductor photocatalysts with narrower band gaps, such as CdS/TiO_2/Pt, TiO_2/Y-Zeolite, Ag_2O/TiO_2, Ag-Bi_2MoO_4, Zeolite/WO_3-Pt, and CdS-SnO_2 with the addition of some oxidant species [21–25].

Several studies related to the synthesis of Fe_2O_3/TiO_2 as a combination of two photocatalysts have been reported [26–29]. The codeposition of noble metals, such as Au, Ag, and Pt, resistant to oxidation or corrosion, on TiO_2, is used as an alternative method to improve the photocatalytic activity of TiO_2 [15,16]. Recently, Mohapatra et al. [30] developed a technique for synthesizing one-dimensional Fe_2O_3/TiO_2 nanorod–nanotube arrays using a pulsed electrodeposition technique. This method provides a multipurpose and useful approach to synthesize one-dimensional heterostructure composites including TiO_2 and other metals for photocatalytic applications or magnetic compounds. Each method has its own strengths and weaknesses. Doping metal or nonmetal onto TiO_2 increases not only the surface area of the photocatalyst but also the crystallinity and molecular structure of the photocatalyst are changed. Some parameters such as specific surface area, crystalline phase, size, and pore distribution are crucial in improving the photocatalytic activity [16,17]. In this study, Ag was used as a dopant because, as a noble metal, it is resistant to oxidation or corrosion. Other noble metals (Au and Pt) are much more expensive compared with Ag. Ag-loaded TiO_2 helps energized electrons to reach to silver and oxygen, rather than positive holes, resulting in restraining the recombination and acting as an electron sink [18–21]. Doped particles are more porous and have higher specific surface area. Doping with silver enhances photocatalytic efficiencies as the band gap is shifted toward the redshift. Ferric oxide (Fe_2O_3) is considered a photocatalyst with the advantages of low cost, nontoxic, and high chemical and physical stability. It has a low band gap energy of 2.2 eV, which can be activated under visible light. Despite its advantages, Fe_2O_3 has drawbacks of the low electrical conductivity and the difficulty to isolate photo-induced electrons and holes to prevent their fast recombination. Therefore, Fe_2O_3 has been considered as an alternative semiconductor to be combined with TiO_2 to improve its photocatalytic activity for the degradation of organic materials.

Extensive attempt has been made to synthesize novel photocatalysts based on TiO_2. Recently some novel photocatalysts were prepared such as Eu/TiO_2/GO [31] and TiO_2/C_3N_4 [32]. Despite some advantages of the photocatalytic method and making new photocatalysts, there are still several limitations that have not been addressed.

In this study, a series of Ag/TiO_2 and Fe_2O_3/TiO_2 photocatalysts at various mass ratios of Ag:TiO_2 and Fe:TiO_2 were synthesized using the novel UV-assisted thermal method, as an alternative approach to conventional individual methods, to improve the photocatalytic activity. Then, the new composite photocatalyst, $Ag/TiO_2/Fe_2O_3$, with a different mass ratio of Ag:TiO_2 and Fe:TiO_2 was synthesized, and the photocatalytic degradation efficiency of aqueous methyl orange (MO) was investigated under UV-A and visible (natural) light. Methyl orange, an azo dye (–N=N–), was selected as the target pollutant for its degradation using the $Ag/TiO_2/Fe_2O_3$ photocatalyst. For the photocatalyst synthesized in our laboratory, its structure ($Ag/TiO_2/Fe_2O_3$), its synthetic method of preparation using UV-assisted thermal technique, and its application in wastewater treatment with high efficiency under sunlight were studied.

1.1. UV-assisted thermal synthesis

There are several methods of synthesis for the metal and nonmetal doping of TiO_2. These methods include sol-gel, hydrothermal, annealing, thermal microwave-assisted, electrochemical anodization, and solvothermal method [5,18,29]. Different doping methods are proposed to enhance the photoactivity of photocatalysts, especially in the range of visible region.

Several factors affect the rate of photochemical reactions such as the concentration of reactants, the temperature, and the light wavelength. UV-C which has a very short wavelength (200–280 nm) can be contemplated as a source of energy that can overcome the activation energy. At high UV light intensity, collisions are more frequent, more particles are activated, and consequently, the speed of reactions will be increased [33]. It has been already confirmed that the high intensity of electron irradiation expressively increases the rate of reactions at lower temperatures for different oxide materials such as $NaFeO_2$, $BaTiO_3$, $NiFe_2O_4$, $LiFe_5O_8$, $MnFe_2O_4$, and $ZnFe_2O_4$ [34]. UV photons are very strong to alter the structure of molecules by breaking down bonds in photolytic reactions, exciting molecules into a higher level of energy (photoexcitation), or ionization of molecules (photo-ionization) [33].

In this study, a novel method of UV-assisted thermal synthesis, as an alternative to conventional methods, was used due to its effectiveness for the enhancement of the photocatalytic activity. This approach is presented to increase the productivity and the latest advances in photocatalytic treatment. UV-C lamps were vertically placed on the exterior of the reactor flask (almost 6 cm far from the flask) to assist the thermal treatment method while minimizing the additional heating requirements. Moussavi et al. [35] reported that UV-C glass tubes are transparent without any phosphorus coating and maximum light emission occurs at 254 nm (85%–90%) and 185 nm (10%–15%), respectively. In brief, the UV-C lamp irradiates light centered at 254 nm because fuse quarts eliminate light centered at 185 nm. To synthesize the novel $Ag/TiO_2/Fe_2O_3$ photocatalyst, the Fe_2O_3/TiO_2 was synthesized followed by silver ion doping onto the combined photocatalysts.

2. Materials and methods

2.1. Materials

All chemicals including tetrabutoxy titanium, ethylene glycol, silver nitrate, ferric nitrate nonahydrate, commercial TiO_2 (rutile, Degussa P25, and anatase), ethanol, and methyl orange were analytical grades, purchased from Sigma-Aldrich (Oakville, ON) and Van Waters and Nat Rogers (VWR, Mississauga, ON). Nitrogen compressed gas, liquid nitrogen, and oxygen compressed gas were analytical

grade and purchased from Linde Canada Industrial gases (Mississauga, ON). All chemicals were used as received.

2.2. Synthesis of Ag-doped TiO_2

There are several methods to synthesize metal-doped TiO_2. In this study, the sol-gel method was utilized because it is the most convenient and important method for synthesis of metal-doped TiO_2. The sol-gel method was performed at ambient pressure, and the procedure is simple and cost-effective with a high yield of production [36,37].

To prepare Ag/TiO_2 based on the sol-gel method, 2.00 g of anatase nano-TiO_2 (prepared using a precursor of tetrabutoxy titanium and ethylene glycol) were weighed and mixed with 50 mL distilled water to make a suspended sol. Then, a stoichiometry amount of $AgNO_3$ was dissolved in distilled water. The silver nitrate solution was added to a flat bottom flask, equipped with a condenser, comprising TiO_2 sol particles suspended in water. The sol-gel thermal-assisted method was used to obtain a higher yield of Ag-doped TiO_2. The composition was mixed and heated at 95°C for at least 24 h by employing a heater-stirrer continuously. The obtained sol-gel was then centrifuged, washed, dried at 105°C, and heated in a muffle furnace at 350°C for 8 h. Based on the stoichiometry of the reaction, the mass ratio of $Ag:TiO_2$ was 0.005. Moreover, the Ag-doped TiO_2 catalysts were synthesized with the mass ratios of $Ag:TiO_2$ = 0.01, 0.05, and 0.1.

2.3. Synthesis of Fe_2O_3/TiO_2

There are several methods for preparing Fe_2O_3/TiO_2 composite photocatalyst. In this study, the Fe_2O_3/TiO_2 photocatalyst was synthesized using the precursor of as-prepared nano-TiO_2, $Fe(NO_3)_3{\cdot}9H_2O$ in ethanol, and applying the UV-assisted thermal synthesis by setting up a glassware reactor at ambient pressure and 90°C. In order to prepare Fe_2O_3/TiO_2 photocatalyst, specific amounts of each precursor were put in a Pyrex flat bottom flask (100 mL). Then, the flask was placed on an electrical heater with magnetic stirrer plate to mix the reactants continuously. The new method of UV-C assisted thermal synthesis was applied to enhance the reaction. Three UV-C lamps (PL-S–9W/TUV-UV Germicide, 110–120V–G23 Base) were placed vertically 6 cm away from the flask. A long glass condenser was used to recover the condensed vapor and return it to the sol-gel. The reaction was set at 90°C in traditional glassware for 5 h to produce the Fe_2O_3/TiO_2 photocatalyst. Samples were centrifuged and dried at 120°C, washed and dried again at 120°C, and then the composite photocatalyst was calcined at 300°C for 4 h. Based on the stoichiometry of the reaction and by applying different amounts of the components, the Fe_2O_3/TiO_2 photocatalyst was prepared with $Fe:TiO_2$ mass ratios of 0.005, 0.01, 0.05, 0.10, and 0.30. Nasirian et al. [6] reported that the best calcination temperature to prepare Fe_2O_3/TiO_2 photocatalyst is in the range 300°C–400°C to achieve a high degradation of organic materials in water. At higher calcination temperatures (over 400°C), anatase is converted to rutile because of Fe^{3+}, which facilitates the conversion. The conversion of anatase to rutile starts at 600°C [38]. In contrast, Pal et al. [39] reported that at the calcination temperature of 500°C, a small amount of rutile starts to be introduced. This fact might be related to the existence of Fe^{3+}, which facilitates the transformation of anatase to a stable form of rutile. Fig. 1(a) shows the actual photos of synthesized Fe_2O_3/TiO_2 photocatalysts with different mass ratios of $Fe:TiO_2$ at various calcination temperatures.

2.4. Synthesis of $Ag/TiO_2/Fe_2O_3$

Two procedures could be used to synthesize the $Ag/TiO_2/Fe_2O_3$ photocatalyst. First, the prepared Fe_2O_3/TiO_2 photocatalyst can react with a silver solution to produce the $Ag/TiO_2/Fe_2O_3$ photocatalyst. In the second method, Ag/TiO_2 is first prepared followed by its reactions with a salt of Fe^{3+}. The percent yield of the production using the second method was lower than that of the first method. In this study, the $Ag/TiO_2/Fe_2O_3$ photocatalyst was synthesized based on the first method using the new preparation method of UV-assisted thermal synthesis. To synthesize the new composite photocatalyst based on the first method, 2.00 g of Fe_2O_3/TiO_2 were added to a flat bottom flask, and then 0.031 g of silver nitrate dissolved in 40 mL of distilled water were added to the flask. The flask was equipped with a long glass condenser to recover the condensed vapor by returning it to the sol-gel flask. Nitrogen gas was continuously injected into the reactants to remove any oxygen from the sol-gel. The mixture

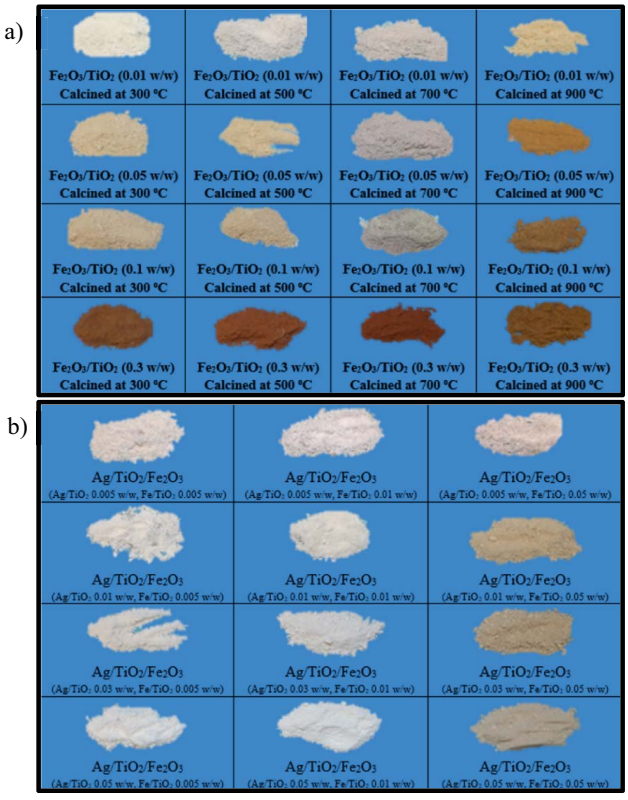

Fig. 1. Actual photos of: (a) synthesized Fe_2O_3/TiO_2 at different calcination temperatures with different mass ratios of $Fe:TiO_2$ ($Fe:TiO_2$ = 0.01, 0.05, 0.1, and 0.30) and (b) synthesized $Ag/TiO_2/Fe_2O_3$ photocatalysts with different mass ratio of $Ag:TiO_2$ and $Fe:TiO_2$.

was heated at 90°C–95°C under continuous magnetic stirring and UV-C irradiation for 12 h. Then, the slurry was cooled to ambient temperature, centrifuged, and washed with water and ethanol to remove nitrate ion. The solid material was then dried at 105°C for 4 h. The product was calcined at 300°C for 6 h. Based on the molecular weight and the stoichiometry of the reaction, the $Ag/TiO_2/Fe_2O_3$ photocatalyst was obtained ($Ag:TiO_2$ = 0.01 w:w and $Fe:TiO_2$ = 0.01 w:w).

Fig. 1(b) shows the actual illustrations of the synthesized $Ag/Fe_2O_3/TiO_2$ photocatalysts with different mass ratios of $Ag:TiO_2$ and $Fe:TiO_2$. It has been shown that at high calcination temperatures of more than 500°C, the photocatalytic activity is significantly decreased due to the phase conversion as well as the reduction in the specific surface area of the photocatalyst [40,41]. At high calcination temperatures, the particle size, the thickness of the crystal, and the degree of crystallinity were increased. This is the main reason that the calcination temperature of all photocatalysts should not exceed the maximum temperature of 300°C.

2.5. Mechanism of photocatalysis

Under the light irradiation with proper energy, an electron in valence band of TiO_2 is promoted to the conduction band. Thus, the negative electron (e^-) and positive hole (h+) pair are formed [5,17,39,40]. During the procedure for oxidative degradation, $HO^\bullet$ radicals are formed which proceed to break down organic molecules. Heterogeneous photocatalytic reactions include complex series of reactions. Agustina et al. [41,42] described some mechanisms of reactions in photocatalysis as follows:

$$h\nu \text{ (light)} + TiO_2 \rightarrow h^+_{vb} + e^-_{cb} \text{ (Light absorption)} \quad (1)$$

$$TiO_2\,(h^+_{vb}) + H_2O_{ads} \rightarrow TiO_2 + H^+ + HO^\bullet \quad (2)$$

$$TiO_2\,(h^+_{vb}) + OH^-_{ads} \rightarrow TiO_2 + HO^\bullet_{ads} \quad (3)$$

$$R\text{–}H + HO^\bullet \rightarrow R^\bullet + H_2O \rightarrow \text{Degradation of pollutants} \quad (4)$$

$$\text{Organic materials} + (TiO_2\text{-}h\nu) \rightarrow \text{Intermediates} \rightarrow CO_2 + H_2O \quad (5)$$

2.6. Analytical techniques and instrumentation

A total organic carbon (TOC) analyzer, Teledyne Tekmar model Apollo 9000, was used to measure concentrations of organics in samples. All water samples were first centrifuged for 30 min at 4,000 rpm (Thermo Scientific Heraeus Multifuge X1, Mississauga, ON). The samples were then filtered by filter papers (VMR Qualitative 410, Mississauga, ON) and were analyzed by the TOC analyzer.

A digital radiometer (DRC-100X, Spectroline, USA) was used to measure the light intensity of the lamps and irradiation sources. The specific surface area of the photocatalyst samples was determined by the Brunauer–Emmet–Teller (BET) method (Quantachrome Nova-e 1200, Burlington, ON) using nitrogen gas, adsorbed at 77 K. For measuring topography, morphology, and structure of the prepared crystals of photocatalysts, scanning electron microscopy (SEM) (JEOL, model JSM-6370 LV, Calgary, AB) with accelerating voltage of 30 keV was used.

Energy dispersive X-ray spectroscopy (EDS) (Oxford Instrument, model X-Max-N-80, Concord, MA), which is coupled with SEM, was employed for elemental analysis. An auto sputter coater (Denton Vacuum Desk IV, Moorestown, NJ) was used for coating samples with a thin layer of gold before analysis by SEM. X-ray diffraction (XRD) model PANalytical X'pert PRO was used to investigate the structure of crystal and conversion phase of photocatalysts. The scanning range of XRD was 10°–100° (2θ).

All instruments were calibrated according to their procedures. All prepared photocatalysts were dried in an oven (Binder, model ED 115-UL). A programmable furnace (Thermo Scientific model Lindberg Blue M) was used for the calcination of samples at different temperatures.

2.7. Experimental setup and procedure

The photocatalytic activities of as-prepared photocatalysts were tested using a batch photoreactor. The experimental setup consisted of a 3.5-L cylindrical glass container for the degradation of organic materials. Five UV-A lamps (9 W, Philips-Actinic BLPL-S, G23 Base) with a maximum peak of 365 nm, were vertically immersed in the photoreactor. The details and the schematic diagram of the experimental setup were already reported in the previous study [5]. The whole photoreactor was placed inside a water container to control the temperature of the photoreactor contents at 25°C using a cooling bath (RTE-211, NESLAB Instruments, Inc., Newington, NH). The photoreactor was placed on a magnetic stirrer so that the contents of the photoreactor were mixed thoroughly during reactions.

3. Results and discussion

3.1. Light intensity

In this study, 9-W artificial UV-A lamps with the maximum light intensity of 365 nm with the light wavelength in the range of 315–400 nm (3.10–3.94 eV) and natural sunlight were used. The sunlight could be utilized as a UV source, but less than 5% of its rays that struck the earth surface are in the wavelength range of 300–400 nm. The effect of the light intensity in the presence of a photocatalyst for the degradation of aqueous MO was investigated in the previous study [5]. The details of the light intensity of UV-A lamp used in this study at different distances from the light source and its comparison with that of the sunlight on a sunny day were reported in the previous study [43]. Result from digital radiometer showed that the light intensity of UV-A lamp varies based on distance of the light source from the detector and the maximum intensity was 14,922 μW/cm² at zero distance, while the maximum intensity of sunlight was 2,140 μW/cm² on a sunny day of summer 2016 at Ryerson University campus at 1:00 p.m. The previous study confirmed that none of the light sources (UV-A and sunlight) had pure spectra and they produced light in a wide range.

3.2. Characterization of $Ag/TiO_2/Fe_2O_3$

Fig. 2(a) shows SEM images of the composite $Ag/Fe_2O_3/TiO_2$ photocatalyst, prepared by the UV-assisted thermal synthesis. The $Ag/TiO_2/Fe_2O_3$ particles displayed a heterogeneous shape and micrometer-sized. Based on the scale of the image, the particle size of the photocatalyst varies between 0.5 and 2.0 μm. Fig. 2(b) shows the results of the EDS for the elemental analysis of the composite $Ag/TiO_2/Fe_2O_3$ photocatalyst ($Ag:TiO_2$ = 0.01 w:w and $Fe:TiO_2$ = 0.05 w:w). Results taken from EDS were in line with the expected concentrations of the elements in the photocatalyst.

The specific surface area of all powder samples was also measured based on the BET method, in which the amount of the adsorbed inert nitrogen gas on the photocatalyst powder was measured. The amount of the adsorbed nitrogen gas corresponds to a monomolecular layer on the surface. Fig. 3 depicts the comparison of the specific surface areas of the prepared composite of $Ag/TiO_2/Fe_2O_3$ photocatalyst with different mass ratios (calcined at 300°C) along with several other commercial photocatalysts. Results show that the commercial rutile has the lowest specific surface area (2.24 m^2/g); whereas, the commercial anatase has the highest specific surface area (42.29 m^2/g) among all bare crystalline forms of TiO_2. This trend correlates with the photocatalytic degradation of MO in the presence of different forms of TiO_2. In heterogeneous photocatalysis, the photocatalytic activity is related to the catalyst species and the amount of metal or nonmetal doped into the catalyst. According to the previous study [6], the highest specific surface area of 98.73 m^2/g for the composite Fe_2O_3/TiO_2 photocatalyst was observed at 0.01 $Fe:TiO_2$ w:w. It is remarkable that the specific surface areas of the bare Fe_2O_3 and anatase were 14.15 and 42.28 m^2/g, respectively. This means that the bare TiO_2 and the bare Fe_2O_3 do not have high specific surface areas, but the combination of these two photocatalysts has a significantly higher specific surface area.

Photocatalytic processes are surface phenomena. A specific surface area is well known as a characteristic for the high activity of a photocatalyst [13]. Based on Langmuir isotherm equation, the degradation of organic materials is proportional to surface-adsorbed reactants [40,44–46]. Based on this equation, the amount of adsorbed pollutants on the surface has a direct relationship to the specific surface area of the photocatalyst. These results confirm that the combination of metal oxide photocatalysts increases the specific surface area, and therefore, the degradation efficiency.

The highest specific surface area of $Ag/TiO_2/Fe_2O_3$ (182.17 m^2/g) was observed at the mass ratios of 0.01 $Ag:TiO_2$ and 0.01 $Fe:TiO_2$, while it was 178.37 m^2/g at the mass ratios of 0.005 $Ag:TiO_2$ and 0.01 $Fe:TiO_2$. Results confirmed that combining two photocatalysts (TiO_2 and Fe_2O_3) followed by their doping with a noble metal (Ag) significantly increased the specific surface area of photocatalysts, adsorption of pollutants, and therefore, their photoactivity. Results also show that by increasing the concentration of iron- and silver-doped into TiO_2, the specific surface area increases and after a specific ratio ($Fe:TiO_2$ = 0.01 w:w and Ag/TiO_2 = 0.01 w:w), it reduces again (see Fig. 3). It seems that at the high concentration of the dopant, the surface of the photocatalyst is entirely covered by the dopant and there is not enough surface area for the photocatalyst to absorb light and generate electrons and holes. Chen et al. [47] reported that F or Ag single-doped (F-TiO_2 or Ag-TiO_2) and codoped F/Ag-TiO_2 photocatalysts (supported by activated carbon) had larger BET surface areas compared with the bare TiO_2 or even TiO_2/activated carbon, which was mainly because of the smaller crystal sizes of the doped photocatalyst. Dandan et al. [48] pointed that the average crystal size of Ce-, N-, or P-doped TiO_2/activated carbon (TiO_2/AC) photocatalyst were smaller compared with that of TiO_2/AC. This synergetic effect of tridoping (Ce, N, and P) is due to higher specific surface area of the photocatalyst, further reducing the crystallite size of photocatalyst. In another study conducted by Tian et al. [49], N-Fe-AC/TiO_2 photocatalyst

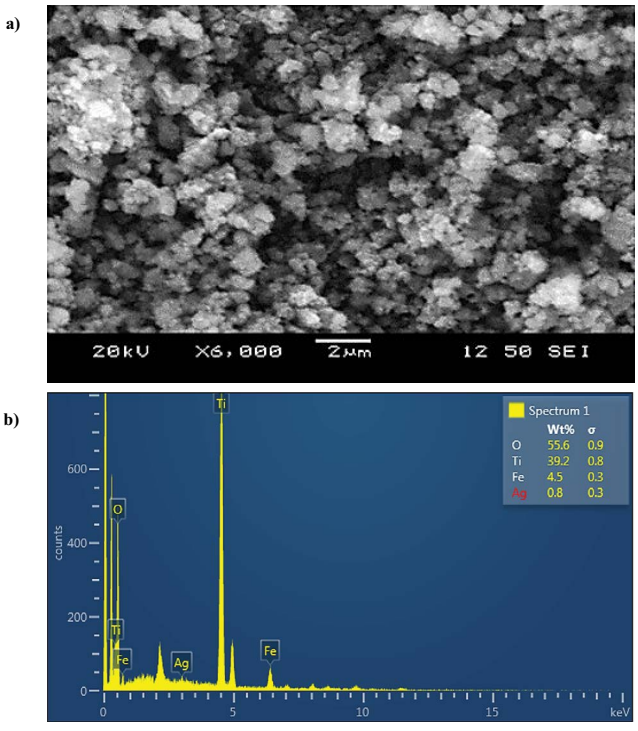

Fig. 2. (a) SEM image of $Ag/TiO_2/Fe_2O_3$ ($Ag:TiO_2$ = 0.01 w:w and $Fe:TiO_2$ = 0.05 w:w) from the whole sample and (b) elemental analysis of the whole sample of $Ag/TiO_2/Fe_2O_3$ ($Ag:TiO_2$ = 0.01 w:w and $Fe:TiO_2$ = 0.05 w:w).

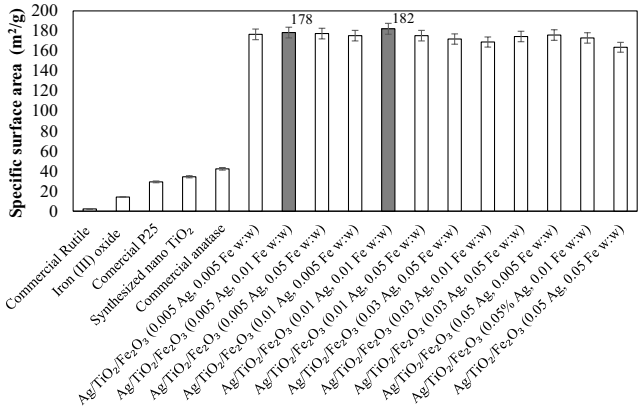

Fig. 3. Comparison of the specific surface area of different photocatalysts. All mass ratios are based on TiO_2.

was synthesized using microwave-assisted sol-gel method. They reported that the spherical shape of codoped N-Fe-AC/TiO_2 photocatalyst has a specific surface area of 550 m^2/g that is much higher than that of the bare TiO_2 and AC/TiO_2.

3.3. Crystallinity of $Ag/TiO_2/Fe_2O_3$ photocatalyst

Although there are numerous reports in the open literature for the preparation of various photocatalysts with different photo-efficiencies to treat organics in wastewater, the configuration and the structure of doped (with metals or nonmetals) and combined photocatalysts are still not clear, and therefore, this needs to be investigated. It is evident that photocatalytic properties are intensively related to several parameters such as the specific surface area, the structure, the size, and the morphology of the crystal. There are two main perspectives, terrestrial and substitution, for doping metals or combining another photocatalyst onto bare TiO_2. The terrestrial is related to the metal/nonmetal covering the surface of the photocatalyst [41,50]; whereas, in the substitution, the metal/nonmetal ions penetrate into the crystal lattice of TiO_2 [37,51,52]. Fig. 4(a) shows a diffractogram (XRD) of the $Ag/TiO_2/Fe_2O_3$ photocatalyst (Ag:TiO_2 = 0.01 w:w and Fe:TiO_2 = 0.01 w:w) which is calcined at 300°C. Results show that the photocatalyst is in the anatase phase with small crystal size, where there is no rutile peak present. Fig. 4(b) shows three diffractograms of $Ag/TiO_2/Fe_2O_3$ with a different mass ratio of Ag^+ and Fe^{3+}, whereas Fig. 4(c) shows diffractograms of the pure commercial anatase. The location of the peaks in the three diffractograms of photocatalysts was in line with that of the pure anatase. According to the Joint Committee on Powder Diffraction Standards (JCPDS-21-1272) databank, anatase has a main peak at 2θ = 25.4 matching the 101 planes and two other peaks located at 37.8 and 48.0 corresponding to planes 004 and 200, respectively [21,38].

Results revealed that all three diffractograms are similar without any alteration in the location of peaks other than their relative heights, which are related to different concentrations of Ag^+ and Fe^{3+}. From these diffractograms, one can conclude that due to the same size of the silver and especially iron ions with titanium, these two ions most likely become parts of the crystal lattice of TiO_2. Substitution of iron or silver into the crystal lattice caused a crystal defect with an increase in the specific surface area of the photocatalyst. Chen et al. [47] and Wellia et al. [51] reported that the metal doped might be placed in the lattice crystal of TiO_2, where it causes some changes in the electronic properties of the photocatalyst. It can be concluded that most of the silver and especially iron ions in the process of doping are substituted with titanium in the crystal lattice of TiO_2 with a low amount of Fe_2O_3 located on the surface of TiO_2. However, the XRD diffractograms show a very low amount of bare Fe_2O_3 particles in the mixed oxide system of the $Ag/TiO_2/Fe_2O_3$ photocatalyst. The XRD patterns show no Ag or Fe species-cause to make a diffraction peaks, it is suggested that Ag or Fe particles are well dispersed onto the TiO_2 crystal lattice or are present in very low amount as iron or silver oxide. Results from other studies [47,51] also confirm the same conclusion.

In our previous study [6], it was found that the best calcination temperature was 300°C for Ag/TiO_2 or combined photocatalysts (Fe_2O_3/TiO_2). It was also found that the sample

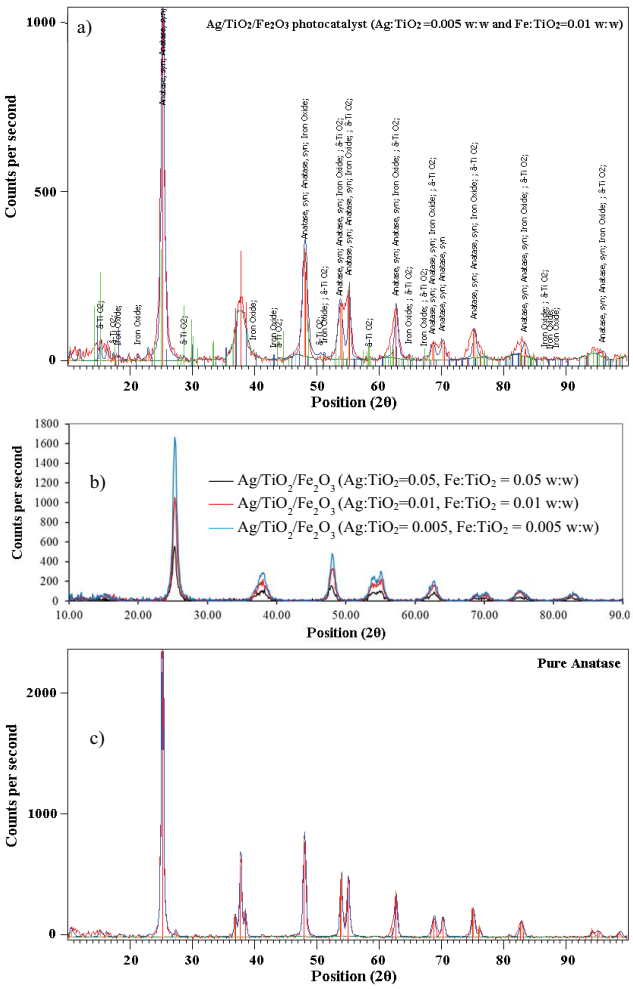

Fig. 4. (a) Diffractogram of the as-prepared $Ag/Fe_2O_3/TiO_2$ photocatalyst (Ag:TiO_2 = 0.005 w:w and Fe/TiO_2 = 0.01 w:w); (b) comparison of three diffractograms (XRD) of $Ag/Fe_2O_3/TiO_2$ with different mass ratios of Ag and Fe; and (c) diffractogram of pure commercial anatase.

calcined at 300°C contained only the anatase form. It has been shown in the open literature that by increasing the calcination temperature, the intensity of anatase peak decreases while the intensity of the rutile peak is amplified [38,39]. At 900°C, there is only the rutile phase with the maximum crystallinity. Results also show that a specific calcination temperature is required to make a purer photocatalyst crystal, whereas, at high calcination temperatures (more than 600°C), the activity of photocatalysts is reduced. It is evident that at high calcination temperatures, the magnetic properties of iron oxides are strongly reduced [21]. Doping TiO_2 with noble metals such as Ag, Au, and Pt increases the photocatalytic activity of the TiO_2 photocatalyst.

Images taken using SEM and result from EDS elemental analysis showed that Ag^+ and Fe^{3+} particles are uniformly dispersed in the mixed oxide samples of $Ag/TiO_2/Fe_2O_3$. In other words, the ratio of atomic percentage of Ag, Ti, and Fe found by EDS are similar to the expected concentrations. At high mass ratios of Fe_2O_3:TiO_2, due to the limitation of solubility of Fe^{3+} ions, the composite photocatalysts contain

an excess Fe_2O_3, which has not been diffused into the TiO_2 lattice. In other words, the excess of Fe_2O_3 in the composite photocatalyst is dispersed on the surface of TiO_2.

3.4. Photocatalytic degradation of methyl orange

In order to determine the adsorption performance of photocatalyst, dark experiments were carried out for all photocatalysts. In this process, the aqueous slurry was stirred in the dark for 180 min to determine the adsorption of methyl orange onto the surface of each photocatalyst and to reach equilibrium between adsorption and desorption of MO. Results showed that equilibrium between adsorption and desorption was obtained after 50 min. In order to examine the photocatalytic activity of all photocatalysts for degradation of MO, under any kind of irradiation (UV-A or sunlight), dark experiments were conducted prior to each run. In the next step, to investigate the photolysis for the degradation of MO in separate experiments, water samples containing MO were exposed to the UV-A irradiation alone and their degradations were monitored. It was observed that by applying photolytic process (only UV-A), a negligible amount of organic materials was degraded after 3 h UV-A irradiation.

The degradation of MO in the presence of several types of commercial bare TiO_2 photocatalysts including rutile, Degussa P25, anatase, and nanosynthesized TiO_2 under UV-A irradiation is shown in Fig. 5(a). It is evident that the range of the MO degradation using bare TiO_2/UV is not high. The best results were obtained in the presence of anatase with the degradation rate of 37.9% after 3 h irradiation. After anatase, nanosynthesized TiO_2 and P25 with almost the same efficiency had the highest, and rutile TiO_2 had the minimum degradation efficiency.

Fig. 5(b) shows the degradation efficiency of MO in the presence of commercial bare Fe_2O_3, bare anatase (TiO_2), and composite Fe_2O_3/TiO_2 with different mass ratios of dopant ($Fe:TiO_2$ = 0.005, 0.01, 0.05, 0.10, and 0.30 w:w). It is evident that the degradation range of MO using bare TiO_2/UV and bare Fe_2O_3/UV for dyes is not high (38.1% and 24.9%, respectively). Fig. 5(b) also shows that the maximum degradation efficiencies of MO in the presence of composite Fe_2O_3/TiO_2 ($Fe:TiO_2$ = 0.01 w:w) reached at 61.5%. This is an improvement of 23.6% compared with the efficiency of bare TiO_2 with 37.9%.

Fig. 5(c) depicts the comparison between the photocatalytic degradation efficiency of MO in the presence of bare anatase (TiO_2), Ag/TiO_2 (synthesized in Sections 2 and 3) with an optimum mass ratio of 0.005 $Ag:TiO_2$ and the composite Fe_2O_3/TiO_2 photocatalyst (with mass ratio of 0.01 $Fe:TiO_2$) under irradiation of UV-A light. Results showed that the degradation of MO reached up to 37.9%, 52.2%, and 61.5%, respectively, which was an improvement in the degradation efficiency of MO. Results from this part of the study confirmed that the doping a noble metal onto TiO_2 (Ag/TiO_2) and combining two photocatalysts (Fe_2O_3/TiO_2) improved the degradation efficiency of the bare TiO_2 photocatalyst.

3.5. Degradation of organics using UV/Ag/TiO_2/Fe_2O_3

Fig. 6(a) shows the photocatalytic degradation of MO using the synthesized $Ag/Fe_2O_3/TiO_2$ photocatalyst under UV-A at

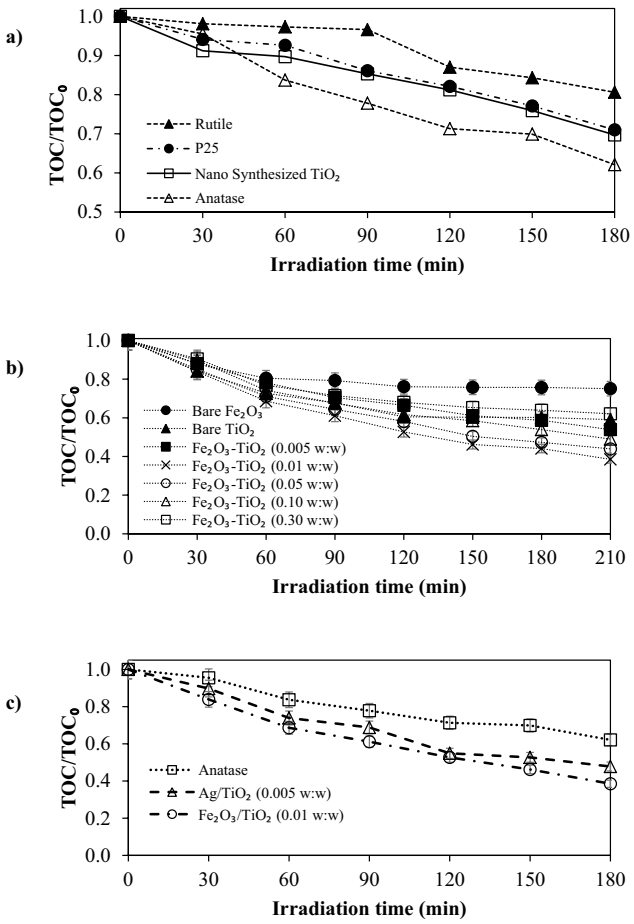

Fig. 5. Comparison in degradation efficiencies of MO in presence of: (a) several types of TiO_2 photocatalysts; (b) commercial Fe_2O_3, bare anatase (TiO_2) and composite Fe_2O_3-TiO_2 with different mass ratios of $Fe:TiO_2$; and (c) anatase TiO_2, Ag-doped TiO_2 (Ag/TiO_2 = 0.05 w:w) and Fe_2O_3/TiO_2 ($Fe:TiO_2$ = 0.01 w:w). The concentration of all photocatalysts was 500 mg/L. The initial concentration of MO was 30 mg/L. Experiments were conducted under irradiation of 5 UV-A in batch mode.

different mass ratios of Ag and Fe to TiO_2 ($Ag:TiO_2$ = 0.01 and $Fe:TiO_2$ = 0.05 w:w; $Ag:TiO_2$ = 0.01 and $Fe:TiO_2$ = 0.01 w:w; and $Ag:TiO_2$ = 0.005 and $Fe:TiO_2$ = 0.01 w:w). The photocatalytic activity of $Ag/TiO_2/Fe_2O_3$ composite photocatalyst is strongly dependent on the mass ratio of Fe and Ag to TiO_2. Results show that the composite photocatalyst of $Ag/TiO_2/Fe_2O_3$ with the mass ratio of 0.005 $Ag:TiO_2$ and 0.01 $Fe:TiO_2$ had the highest photocatalytic activity for the degradation of MO (79.5%) in aqueous solutions.

Results also show that the degradation efficiency of the $Ag/TiO_2/Fe_2O_3$ at the optimum mass ratio was higher than that of Fe_2O_3/TiO_2 at its optimum amount mass ratio and that of bare TiO_2. The high amount of silver or iron loadings onto the TiO_2, beyond the optimum level, decreases the available surface area for the adsorption of organic materials and blocks the light absorption, consequently a decrease in the photocatalytic activity. Based on the photo-generation of electron/hole pair in photocatalysts, the electron is reducer and the hole is an oxidizer. Although holes are oxidizers

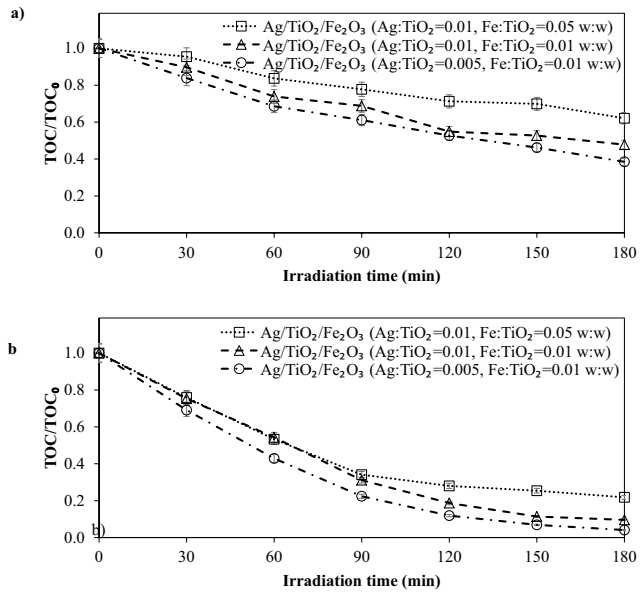

Fig. 6. Degradation of methyl orange in the presence of composites of $Ag/Fe_2O_3/TiO_2$ photocatalyst at different mass ratios of Fe and Ag under: (a) UV-A 45W and (b) natural sunlight irradiation. The concentration of photocatalyst in each case was 500 mg/L.

and produce hydroxyl radicals, oxygen molecules in water samples scavenge electrons generated from the photoactivation of catalysts; thus, several kinds of superoxides are produced. Subsequently, superoxides in a series of reactions react with water and produce hydroxyl radicals.

According to Yang et al. [53] and based on results obtained from thermal desorption spectroscopy, in combined photocatalysts, O_2^-, O^-, and O_3^- can be adsorbed on the surface of photocatalysts and then desorb at high temperature (114°C). The rate of adsorption of oxygen on the surface of combined photocatalysts is higher than that of bare photocatalysts. High adsorption of superoxide causes a higher degradation of organics. Kim et al. [21] reported that in the XPS analysis of combined Fe_2O_3/TiO_2 photocatalyst (calcined at 700°C), a separate peak related to the oxygen vacancies was obtained. Oxygen defects cause an increase in the photocatalytic activity of Fe_2O_3/TiO_2. They suggested a mechanism based on trapping of water molecules by oxygen vacancies and then by the dissociation of the adsorbed water into O_2^-, H_2O_2, and $HO^\bullet$. Consequently, the enhancement of the photocatalytic activity of the $Ag/TiO_2/Fe_2O_3$ photocatalyst is mainly attributed to the titanium and oxygen defects in the crystal and to the modification of the electronic structure of TiO_2, which can reduce the recombination rate of electron/hole pairs and reduce the band gap energy.

Fig. 6(b) shows the degradation efficiency of the $Ag/TiO_2/Fe_2O_3$ photocatalyst with different mass ratios under natural sunlight. The highest amount of the MO degradation was reached to 95.6%. In other words, the photocatalyst absorbed visible light to generate electron/hole pairs to degrade organic materials, which means a redshift occurred. Another advantage of applying the $Ag/TiO_2/Fe_2O_3$ photocatalyst is its easy separation from the slurry due to its electromagnetic characteristic of $Ag/TiO_2/Fe_2O_3$. This separation is easily performed by applying a proper electromagnetic field or, at least, applying a ferromagnetic material and passing suspension through the field. Sequential runs were carried out four times to determine the stability and reusability of the novel photocatalyst. Results showed that the degradation efficiency of MO was almost the same; in other words, there was no failure in the reuse of the photocatalyst.

4. Conclusions

Doping transition metals onto TiO_2 and the combination of two semiconductor oxides are two appropriate alternatives to improve photocatalytic activity of the bare TiO_2 in order to degrade organics. This could change the electronic structure and the band gap energy of the main photocatalyst. To get past current restrictions on the fast rate of electron–hole recombination, the $Ag/TiO_2/Fe_2O_3$ photocatalyst was synthesized to improve the photocatalytic activity of TiO_2. The new composite of $Ag/TiO_2/Fe_2O_3$ was synthesized by the novel UV-assisted thermal method as an alternative to enhance the generation and the lifetime of electron/hole pairs as well as to improve its photocatalytic activity for the degradation of an azo dye. Results showed that combining two photocatalysts (TiO_2 and Fe_2O_3) and then doping silver ion onto combined photocatalysts caused the substitution impurity and point defect in the crystal.

The diffractogram of $Ag/TiO_2/Fe_2O_3$ with different concentration of dopant (Ag and Fe) calcined at 300°C showed that all photocatalysts were in anatase form. Results also showed that the degradation of methyl orange using $Ag/TiO_2/Fe_2O_3$ ($Ag:TiO_2$ = 0.005 w:w and $Fe:TiO_2$ = 0.01 w:w) was reached to 89.5% under UV-A irradiation and 95.6% under natural sunlight. In other words, the degradation efficiency of MO was significantly increased, especially under natural sunlight. Results showed that the combination of crystal defect, higher specific surface area, higher adsorption of organics, lower band gap energy, and consequently the effect of redshift caused to improve the photocatalytic activity.

Acknowledgment

The financial support of the Natural Sciences and Engineering Research Council of Canada (NSERC), Ontario Graduate Scholarship (OGS), and Ryerson University Faculty of Engineering and Architectural Science Dean's Research Fund is greatly appreciated.

References

[1] M. Visa, F. Pricop, A. Duta, Sustainable treatment of wastewaters resulted in the textile dyeing industry, Clean Technol. Environ. Policy, 13 (2011) 855–861.
[2] F.V. De Andrade, G.M. De Lima, R. Augusti, M.G. Coelh, J.D. Ardisson, O.B. Romero, A versatile approach to treat aqueous residues of textile industry: the photocatalytic degradation of Indigo Carmine dye employing the autoclaved cellular concrete/Fe_2O_3 system, Chem. Eng. J., 180 (2012) 25–31.
[3] M. Mohajerani, M. Mehrvar, F. Ein-Mozaffari, Correlation and prediction of azo dye degradation by nonlinear least-square regression in combined ozonation and ultrasonolysis processes, Water Qual. Res. J. Can., 46 (2011) 250–258.

[4] M. Mohajerani, M. Mehrvar, F. Ein-Mozaffari, Degradation of aqueous methylene blue using an external loop airlift sonophotoreactor: statistical analysis and optimization, J. Environ. Sci. Health Part A Toxic/Hazard. Subst. Environ. Eng., 51 (2016) 722–735.
[5] M. Nasirian, M. Mehrvar, Modification of TiO_2 to enhance photocatalytic degradation of organics in aqueous solutions, J. Environ. Chem. Eng., 4 (2016) 4072–4082.
[6] M. Nasirian, C.F. Bustillo-Lecompte, M. Mehrvar, Photocatalytic efficiency of Fe_2O_3/TiO_2 for the degradation of typical dyes in textile industries: effects of calcination temperature and UV-assisted thermal synthesis, J. Environ. Manage., 196 (2017) 487–498.
[7] D. Hamad, M. Mehrvar, R. Dhib, Experimental study of polyvinyl alcohol degradation in aqueous solution by UV/H_2O_2 process, Polym. Degrad. Stabil., 103 (2014) 75–82.
[8] D. Hamad, R. Dhib, M. Mehrvar, Photochemical degradation of aqueous polyvinyl alcohol in a continuous UV/H_2O_2 process: experimental and statistical analysis, J. Polym. Environ., 24 (2016) 72–83.
[9] A. Mowla, M. Mehrvar, R. Dhib, Combination of sonophotolysis and aerobic activated sludge processes for treatment of synthetic pharmaceutical wastewater, Chem. Eng. J., 255 (2014) 411–423.
[10] C.F. Bustillo-Lecompte, M. Mehrvar, Treatment of an actual slaughterhouse wastewater by integration of biological and advanced oxidation processes: modeling, optimization, and cost-effectiveness analysis, J. Environ. Manage., 182 (2016) 651–666.
[11] C.F. Bustillo-Lecompte, M. Knight, M. Mehrvar, Assessing the performance of UV/H_2O_2 as a pretreatment process in TOC removal of an actual petroleum refinery wastewater and its inhibitory effects on activated sludge, Can. J. Chem. Eng., 93 (2015) 798–807.
[12] C.F. Bustillo-Lecompte, S. Ghafoori, M. Mehrvar, Photochemical degradation of an actual slaughterhouse wastewater by continuous UV/H_2O_2 photoreactor with recycle, J. Environ. Chem. Eng., 4 (2016) 719–732.
[13] U.G. Akpan, B.H. Hameed, Parameters affecting the photocatalytic degradation of dyes using TiO_2-based photocatalysts: a review, J. Hazard. Mater., 170 (2009) 520–529.
[14] S.I. Shah, W. Li, C.P. Huang, O. Jung, C. Ni, Study of Nd_3^+, Pd_2^+, Pt_4^+, and Fe_3^+ dopant effect on photoreactivity of TiO_2 nanoparticles, Proc. Natl. Acad. Sci. U.S.A., 99 (2002) 6482–6486.
[15] L. Zhang, T. Kanki, N. Sano, A. Toyoda, Development of TiO_2 photocatalyst reaction for water purification, Sep. Purif. Technol., 31 (2003) 105–110.
[16] J. Bandara, R.A.S.S. Ranasinghe, The effect of MgO coating on photocatalytic activity of SnO_2 for the degradation of chlorophenol and textile colorants; the correlation between the photocatalytic activity and the negative shift of flatband potential of SnO_2, Appl. Catal., A, 319 (2007) 58–63.
[17] Y. Cao, H. Tan, T. Shi, T. Tang, J. Li, Preparation of Ag-doped TiO_2 nanoparticles for photocatalytic degradation of acetamiprid in water, J. Chem. Technol. Biotechnol., 83 (2008) 546–552.
[18] B. Gao, T.M. Lim, D.P. Subagio, T.T. Lim, Zr-doped TiO_2 for enhanced photocatalytic degradation of bisphenol A, Appl. Catal., A, 375 (2010) 107–115.
[19] E. Grabowska, J. Reszczyńska, A. Zaleska, Mechanism of phenol photodegradation in the presence of pure and modified-TiO_2: a review, Water Res., 46 (2012) 5453–5471.
[20] L.G. Devi, R. Kavitha, A review on nonmetal ion doped titania for the photocatalytic degradation of organic pollutants under UV/solar light: role of photogenerated charge carrier dynamics in enhancing the activity, Appl. Catal., B, 140–141 (2013) 559–587.
[21] Y. Kim, K. Jung, J.Y. Hwang, S. Ahn, K.Y. Kwon, Photocatalytic property of nitrogen and nickel codoped titanium oxides, Bull. Korean Chem. Soc., 37 (2016) 1768–1771.
[22] V. Etacheri, C. Di Valentin, J. Schneider, D. Bahnemann, S.C. Pillai, Visible-light activation of TiO_2 photocatalysts: advances in theory and experiments, J. Photochem. Photobiol., C, 25 (2015) 1–29.
[23] D. Sudha, P. Sivakumar, Review on the photocatalytic activity of various composite catalysts, Chem. Eng. Process., 97 (2015) 112–133.
[24] R. Fagan, D.E. McCormack, D.D. Dionysiou, S.C. Pillai, A review of solar and visible light active TiO_2 photocatalysis for treating bacteria, cyanotoxins and contaminants of emerging concern, Mater. Sci. Semicond. Process., 42 (2016) 2–14.
[25] P.A.K. Reddy, P.V.L. Reddy, E. Kwon, K.H. Kim, T. Akter, S. Kalagara, Recent advances in photocatalytic treatment of pollutants in aqueous media, Environ. Int., 91 (2016) 94–103.
[26] Y. Shaogui, Q. Xie, L. Xinyong, L. Yazi, C. Shuo, C. Guohua, Preparation, characterization and photoelectrocatalytic properties of nanocrystalline Fe_2O_3/TiO_2, ZnO/TiO_2, and Fe_2O_3/ZnO/TiO_2 composite film electrodes towards pentachlorophenol degradation, Phys. Chem. Chem. Phys., 6 (2004) 659–664.
[27] H. Zhang, X. Wu, Y. Wang, X. Chen, Z. Li, T. Yu, J. Ye, Z. Zou, Preparation of $Fe_2O_3/SrTiO_3$ composite powders and their photocatalytic properties, J. Phys. Chem. Solids, 68 (2007) 280–283.
[28] T.K. Ghorai, M. Chakraborty, P. Pramanik, Photocatalytic performance of nano-photocatalyst from TiO_2 and Fe_2O_3 by mechanochemical synthesis, J. Alloys Compd., 509 (2011) 8158–8164.
[29] M. Nasirian, Y.P. Lin, C.F. Bustillo-Lecompte, M. Mehrvar, Enhancement of photocatalytic activity of titanium dioxide using non-metal doping methods under visible light: a review, Int. J. Environ. Sci. Technol., 15 (2018) 2009–2032.
[30] S.K. Mohapatra, S. Banerjee, M. Misra, Synthesis of Fe_2O_3/TiO_2 nanorod–nanotube arrays by filling TiO_2 nanotubes with Fe, Nanotechnology, 19 (2008) 315601–315607.
[31] Y. Jiaying, T. Jie, Z. Xiuhui, J. Xinyu, J. Feipeng, Y. Jingang, Synthesis, characterization and photocatalytic activities of a novel Eu/TiO_2/GO composite, and its application for enhanced photocatalysis of methylene blue, Nanosci. Nanotechnol. Lett., 9 (2017) 1622–1631.
[32] M. Reli, P. Huo, M. Šihor, N. Ambrožová, I. Troppová, L. Matějová, J. Lang, L. Svoboda, P. Kusťrowski, M. Ritz, P. Praus, K. Kocí, Novel TiO_2/C_3N_4 photocatalysts for photocatalytic reduction of CO_2 and for photocatalytic decomposition of N_2O, J. Phys. Chem., 120 (2016) 8564–8573.
[33] S. Ranjan, D.D. Sasselov, Influence of the UV environment on the synthesis of prebiotic molecules, Astrobiology, 16 (2016) 68–88.
[34] A.P. Surzhikov, E.A. Vasendina, E.N. Lysenko, E.V. Nikolaev, Kinetics of phase formation in a Li_2CO_3-TiO_2-Fe_2O_3 system during radiation-thermal synthesis, Inorg. Mater., 5 (2014) 102–106.
[35] G. Moussavi, M. Pourakbar, E. Aghayani, M. Mahdavianpour, S. Shekoohyian, Comparing the efficacy of VUV and UVC/$S_2O_8^{2-}$ advanced oxidation processes for degradation and mineralization of cyanide in wastewater, Chem. Eng. J., 294 (2016) 273–280.
[36] B. Tryba, A.W. Morawski, M. Inagaki, M. Toyoda, Effect of the carbon coating in Fe-C-TiO(2) photocatalyst on phenol decomposition under UV irradiation via photo-Fenton process, Chemosphere, 64 (2006) 1225–1232.
[37] N. Nasralla, M. Yeganeh, Y. Astuti, S. Piticharoenphun, N. Shahtahmasebi, A. Kompany, M. Karimipour, B.G. Mendis, N.R.J. Poolton, L. Šiller, Structural and spectroscopic study of Fe-doped TiO_2 nanoparticles prepared by sol-gel method, Sci. Iran, 20 (2013) 1018–1022.
[38] S. Dai, Y. Wu, T. Sakai, Z. Du, H. Sakai, M. Abe, Preparation of highly crystalline TiO_2 nanostructures by acid-assisted hydrothermal treatment of hexagonal-structured nanocrystalline titania/cetyltrimethyammonium bromide nanoskeleton, Nanoscale Res. Lett., 5 (2010) 1829–1835.
[39] B. Pal, M. Sharon, G. Nogami, Preparation and characterization of TiO_2/Fe_2O_3 binary mixed oxides and its photocatalytic properties, Mater. Chem. Phys., 59 (1999) 254–261.
[40] M. Hamadanian, A. Reisi-Vanani, A. Majedi, Synthesis, characterization and effect of calcination temperature on phase transformation and photocatalytic activity of Cu, S-codoped TiO_2 nanoparticles, Appl. Surf. Sci., 256 (2010) 1837–1844.
[41] T.E. Agustina, H.M. Ang, V.K. Vareek, A review of synergistic effect of photocatalysis and ozonation on wastewater treatment, J. Photochem. Photobiol., C, 6 (2005) 264–273.
[42] T.E. Agustina, H.M. Ang, V.K. Pareek, Treatment of winery wastewater using a photocatalytic/photolytic reactor, Chem. Eng. J., 135 (2008) 151–156.

[43] M. Nasirian, M. Mehrvar, Photocatalytic degradation of aqueous Methyl Orange using nitrogen doped TiO_2 photocatalyst prepared by novel method of UV assisted thermal synthesis, J. Environ. Sci., 66 (2018) 81–93.
[44] B. Mazinani, A.K. Masrom, A. Beitollahi, R. Luque, Photocatalytic activity, surface area and phase modification of mesoporous SiO_2–TiO_2 prepared by a one-step hydrothermal procedure, Ceram. Int., 40 (2014) 11525–11532.
[45] Q.Z. Yan, X.T. Su, Z.Y. Huang, C.C. Ge, Sol–gel auto-igniting synthesis and structural property of cerium-doped titanium dioxide nanosized powders, J. Eur. Ceram. Soc., 26 (2006) 915–921.
[46] F. Amano, K. Nogami, M. Tanaka, B. Ohtani, Correlation between surface area and photocatalytic activity for acetaldehyde decomposition over bismuth tungstate particles with a hierarchical structure, Langmuir, 26 (2010) 7174–7180.
[47] X. Chen, D. Liu, Z. Wu, G. Cravotto, Z. Wu, B.-C. Ye, Microwave-assisted rapid synthesis of Ag-β-cyclodextrin/TiO_2 /AC with exposed {001} facets for highly efficient naphthalene degradation under visible light, Catal. Commun., 104 (2018) 96–100.
[48] L. Dandan, L. Yiming, W. Zhansheng, T. Fei, Y. Bang-Ce, C. Xiaoqing, Enhancement of photodegradation of Ce, N, and P tri-doped TiO_2/AC by microwave radiation with visible light response for naphthalene, J. Taiwan Inst. Chem. Eng., 68 (2016) 506–513.
[49] F. Tian, Z. Wu, Y. Tong, Z. Wu, G. Cravotto, Microwave-assisted synthesis of carbon-based (N, Fe)-codoped TiO_2 for the photocatalytic degradation of formaldehyde, Nanoscale Res. Lett., 10 (2015) 360–371.
[50] H. Liu, X. Dong, L. Nan, H. Ma, X. Chen, Z. Zhu, A novel fabrication of silver-modified TiO_2 colloidal-assembled microstructures and enhanced visible photocatalytic activities, Mater. Lett., 159 (2015) 142–145.
[51] D.V. Wellia, Q.C. Xu, M.A. Sk, K.H. Lim, T.M. Lim, T.T.Y. Tan, Experimental and theoretical studies of Fe-doped TiO_2 films prepared by peroxo sol-gel method, Appl. Catal., A, 401 (2011) 98–105.
[52] A. Banisharif, A.A. Khodadadi, Y. Mortazavi, A. Anaraki Firooz, J. Beheshtian, S. Agah, S. Menbari, Highly active Fe_2O_3-doped TiO_2 photocatalyst for degradation of trichloroethylene in air under UV and visible light irradiation: experimental and computational studies, Appl. Catal., B, 165 (2015) 209–221.
[53] J. Yang, L. Li, Z. Zhang, Q. Li, H. Wang, A study of the photocatalytic oxidation of formaldehyde on Pt/Fe_2O_3/TiO_2, J. Photochem. Photobiol., A, 137 (2000) 197–202.